[33]D. R. O. Morrison, Phys. Letters 22, 528 (1966).
[34]See, for example, C. W. Akerlof *et al.*, Phys. Rev. Letters 27, 539 (1971).
[35]Further, if two single particles were exchanged the amplitudes could have an interference which could lead to a polarization of the Λ from the $\Sigma^-(1385)$ decay. However, there are too few events in our data to obtain reliable polarization information.
[36]An experimental comment is in order here. Since the reaction $K^-p \to \Lambda\pi^-\pi^+$ is dominated by $\Sigma(1385)^+$ as well as ρ^0, f^0, etc., a missing-mass search for $\Sigma(1385)^-$ by detecting π^+ *only* from the reaction $K^-p \to \pi^+ +$ anything is probably fruitless; also the production cross section of $\Sigma(1385)^-$ is small and the possible signal will be buried under overwhelming reflections from other strongly produced resonances as stated above. This, certainly, is the case for the reaction $\pi^-p \to K^+\Lambda\pi^-$ investigated in this experiment.

PHYSICAL REVIEW D VOLUME 6, NUMBER 5 1 SEPTEMBER 1972

K^+ Decay in Flight*

I-H. Chiang, J. L. Rosen,† and S. Shapiro
University of Rochester, Rochester, New York 14627

and

R. Handler, S. Olsen,‡ and L. Pondrom§
University of Wisconsin, Madison, Wisconsin 53706
(Received 5 May 1972)

From a sample of 10^5 K^+ decays in flight the following branching ratios were obtained: $K_{\mu 2} = (63.24 \pm 0.44)\%$, $K_{\pi 2} = (21.18 \pm 0.28)\%$, $\tau(K^+ \to \pi^+\pi^+\pi^-) = (5.56 \pm 0.20)\%$, $\tau'(K^+ \to \pi^+\pi^0\pi^0) = (1.84 \pm 0.06)\%$, $K_{\mu 3} = (3.33 \pm 0.16)\%$, and $K_{e3} = (4.86 \pm 0.10)\%$. The phase-space distributions for three-body semileptonic modes were studied in detail from a second sample of 10^5 decays. For 4017 $K^+ \to \pi^0 e^+ \nu$ events, $\lambda_+ = 0.029 \pm 0.011$. Limits on scalar and tensor form factors of $|f_S/f_+| < 0.13$ and $|f_T/f_+| < 0.75$ (90% confidence) were obtained. For $K^+ \to \pi^0\mu^+\nu$ a parametrized fit to 3900 events assuming $\lambda_+ = \lambda_- = +0.030$ gave $\xi = -0.09 \pm 0.28$.

I. EXPERIMENTAL ARRANGEMENT

The subject of K^+ decays has been thoroughly reviewed in the literature.[1-3] The experiment discussed here was designed to study the decay of 1.84-GeV/c K^+'s in flight, with emphasis placed on good detection efficiency for γ rays from π^0 decay and a minimum of kinematic bias. Optical spark chambers were used to observe the decay products. The technique of using in-flight decay to measure properties in the K^+ rest frame offers certain technical advantages which are worth special mention. The velocity of the decaying system in the laboratory compacts the decay products into a forward cone, and increases their kinetic energy. All of the dominant decay modes of the K^+ except $(\mu^+\nu)$ and $(\pi^+\pi^+\pi^-)$ contain at least one π^0 in the final state. A high-average π^0 energy results in a sample of predominantly well-collimated and high-energy γ rays, which can be detected with better efficiency than the 100-MeV γ rays resulting from K^+ decay at rest. The muons from the decay $(\mu^+\pi^0\nu)$ have an average energy around 500 MeV, and therefore a range of about two collision lengths, which can be advantageous in π^+-μ^+ separation. Furthermore, the K^+ decay can occur in a very-low-density medium – essentially a gas at atmospheric pressure – leading to a good vertex determination and low multiple scattering of the charged secondaries.

The experimental setup is shown in Fig. 1. The 1.84-GeV/c K^+ mesons were obtained in a partially separated beam at the Argonne Zero Gradient Synchrotron (ZGS). The K^+ flux was intentionally

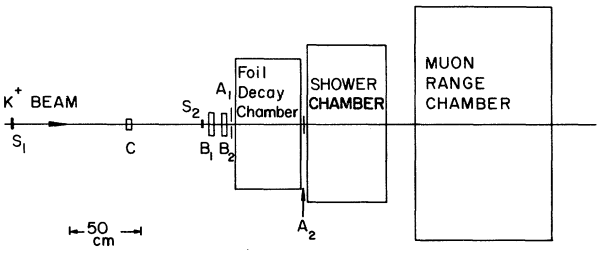

FIG. 1. Plan view of the apparatus. The enriched K^+ beam at 1.84 GeV/c was defined by scintillators S_1, S_2 and the liquid cell differential Cherenkov counter C. B_1 and B_2 were beam spark chambers. The decay volume was defined by the hole veto counter A_1 and the beam veto counter A_2. The dimensions and properties of the spark chambers are given in the text.

kept low, about 300 K^+/pulse over a 600-msec spill. The π^+/K^+ ratio was 10/1. Therefore the total charged-particle flux through the apparatus was only a few thousand particles per second. A liquid differential Cherenkov counter was used to identify K^+ mesons in the beam, and the K^+ entering the decay volume was defined by a veto counter A_1 with a 1.5-cm-diameter hole. The spark chambers were triggered if the K^+ failed to strike the 6.35-cm-diameter veto counter A_2 placed 57 cm (0.04 decay lengths) from A_1. This very loose trigger ensured a minimum of bias in the K^+ decay events obtained. Camera dead time limited the event rate to 4/pulse. Different types of spark chambers were used to identify various components of K^+ decay. Upstream of A_1 two foil chambers (B_1 and B_2) were used to measure the incident K^+ direction. The decay chamber, between A_1 and A_2, had 40 gaps 1.3 cm wide with 15-μ-thick aluminum foils serving as spark-chamber plates. This region presented 3.0×10^{-3} interaction lengths to the K^+ beam, approximately 80% of which was due to the foils and 20% due to the neon gas. The amount of material here was kept small to minimize both multiple scattering and the probability of the K^+ interacting rather than decaying. Downstream of the decay chamber, immediately behind A_2, was the shower chamber for the conversion of the $\pi^0\gamma$ rays. It was composed of 66 stainless steel plates each 0.09 radiation lengths thick. This chamber was 1.2×1.2 m in transverse dimension, subtending a half-angle of 35° at the center of the decay path. Further downstream twenty 2.5-cm-thick steel plates 1.8×1.8 m in transverse dimension were used to stop muons with kinematic energy less than 0.8 GeV. Thin-plate two-gap spark chambers were placed between each plate of steel to observe the muon range. Each event was photographed by a single 35-mm camera viewing the chamber array in 90° stereo.

In the course of a three week run, 10^6 events were recorded on film. Because of the low flux

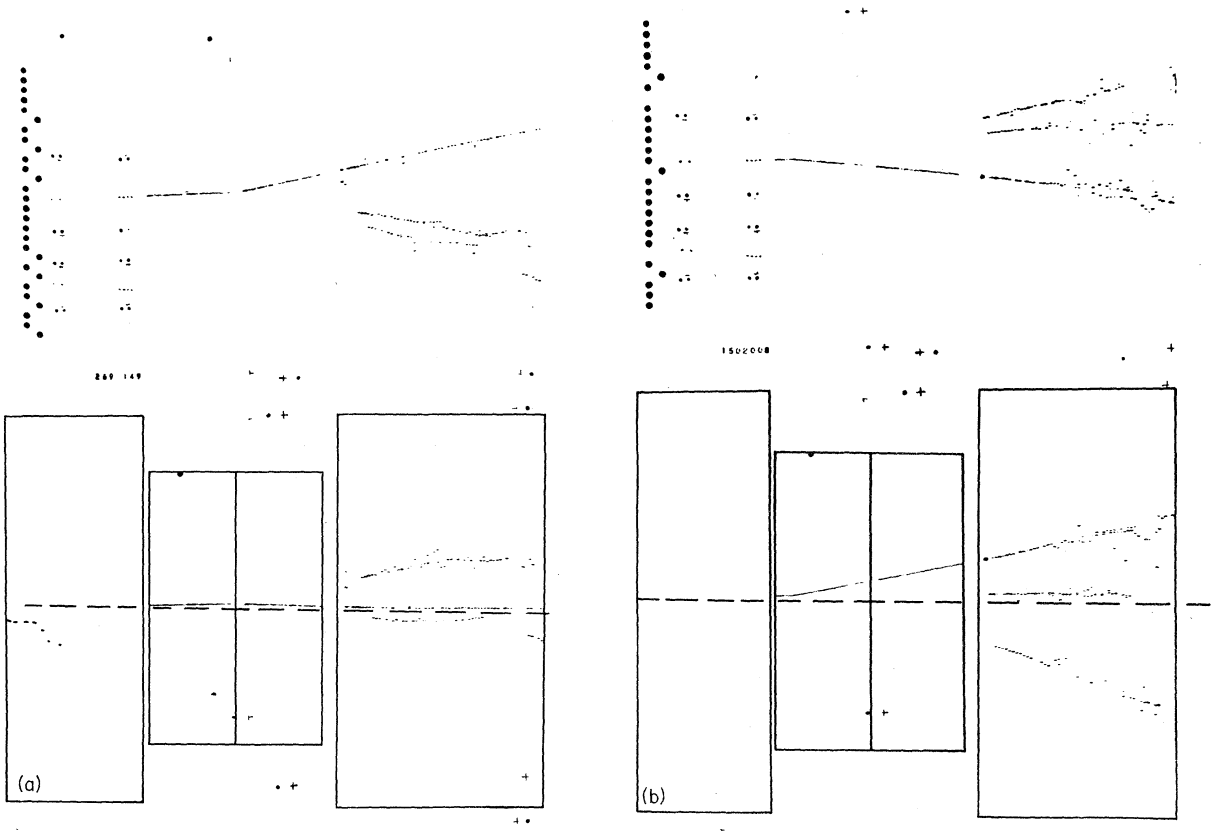

FIG. 2. (a) Typical $K_{\mu3}$ candidate event, characterized by a kink + 2 γ rays. The chamber outlines are shown in the side view. The foil chamber was built in two modules. The beam chambers were viewed in 90° stereo in the top view of the apparatus. The muon range chamber was physically downstream of the shower chamber, but was optically placed upstream, and was observed only in the side view. The other chambers were observed in 90° stereo. (b) Typical K_{e3} candidate event, where the charged particle track produces an electromagnetic shower.

TABLE I. Scanning summary based on 97 967 events.

Category	Decay mode	Topology of decay	Percent of K events	Number of events
$K_{\mu 2}$	$\mu^+\nu$	Single charged-particle kink	64.4	63 110
$4\gamma\tau'$	$\pi^+\pi^0\pi^0$	Single kink plus 3 or 4 γ-ray showers	0.70	691
$3\gamma\tau'$	$\pi^+\pi^0\pi^0$		0.63	616
τ	$\pi^+\pi^+\pi^-$	3 charged particles	2.4	2330
$2\gamma K_{e3}$	$e^+\pi^0\nu$	Charged particle shower plus two γ rays	3.6	3539
$2\gamma K_{\pi 2}$	$\pi^+\pi^0$	Charged particle star in shower chamber + two γ's (π^*)	3.9	3798
$2\gamma K_{\mu 3}$	$(\pi^+\pi^0)+(\mu^+\pi^0\nu)$	Straight charged secondary and two γ's	15.2	14 890
K^+ foil	Interaction of K^+ in decay vol.	Recoil observed	2.6	2577
1γ	all modes with π^0	Charged particle + 1γ shower	6.2	6108
0γ	$\pi^+\pi^0$ and $e^+\pi^0\nu$	Charged particle shower or star with no γ rays	0.3	308
		Total	99.9%	97 967

of charged particles through the detector, the multiple track and background rates were small, and the film was quite clean. Approximately 75% of the film consisted of single-event triggers, either K^+ decays or K^+ interactions within the fiducial region between A_1 and A_2.

II. DATA REDUCTION - BRANCHING RATIOS

The film was scanned and each K^+ decay event was classified according to its topology.[4] Event classification was based on the number of visible γ-ray conversions and the appearance of the charged secondary. A straight charged secondary was considered a μ-candidate; a charged track which produced a shower was considered a positron. A typical "kink + 2γ" event is shown in Fig. 2(a) and a "$2\gamma e$" event in Fig. 2(b). Table I shows the results of the classification of 97 967 events according to their appearance on the scanning table. The high probability for γ-ray detection in the setup can be seen from the fact that of all events with at least one γ ray, 80% had two or more, and from the fact the numbers of 3γ and 4γ $\pi^+\pi^0\pi^0$ events were essentially equal. Except at low energies, below 100 MeV, the showers pointed quite well towards the decay vertex. To be called a γ-ray conversion, a shower had to show at least 4 sparks in 5 gaps in the shower chamber on the scan table. This gave a very rough lower energy cutoff of around 50 MeV. Approximately 20% of the charged pions incident on the shower chamber made a nuclear interaction in one of the steel plates with visible secondaries, and hence identified themselves as pions (called π^*). The remainder of the pions could not be distinguished from muons on the scanning table. In order to minimize the sensitivity to the precise location of the veto counter A_2, decay vertices were restricted to the first 28 cm of decay path. The decay mode categorization by scanning was fairly complete with only small correction necessary between the various modes once a separation of the $K_{\pi 2}$ and $K_{\mu 3}$ events was achieved. It is worth noting that the $\pi^+\pi^+\pi^-(\tau)$ mode was suppressed in the data relative to the other modes

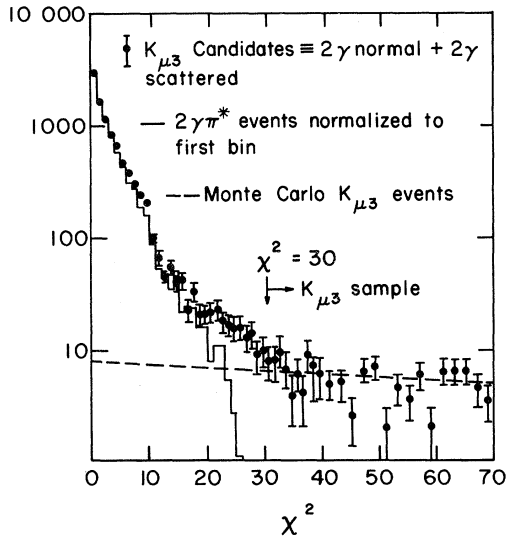

FIG. 3. Two-body χ^2 curve for the $K_{\mu 3}$ candidates. The solid histogram is from $K_{\pi 2}$ events where the π^+ could be positively identified by a nuclear reaction in the thin steel plates of the shower chamber, normalized to the peak value. The dashed curve is the Monte Carlo result expected for $K_{\mu 3}$ events.

TABLE II. Branching ratio.

Mode	Number of events	Detection efficiency	Percentage error	Branching ratio %	1971 average % [a]
$K_{\mu 2}$	62 144	0.9181	0.7%	63.24± 0.44	63.77± 0.28
$K_{\pi 2}$	16 187	0.7141	1.3%	21.18± 0.28	20.92± 0.29
τ	2330	0.3918	3.6%	5.56± 0.20	5.58± 0.030
τ'	1307	0.6630	3.1%	1.84± 0.06	1.677± 0.044
$K_{\mu 3}$	2345	0.659	4.9%	3.33± 0.16	3.20± 0.11
K_{e3}	3516	0.6763	2.1%	4.86± 0.10	4.85± 0.07

[a] See Ref. 3.

with only one charged particle in the final state because it was difficult for all three charged secondaries to miss the veto A_2.

Each event in the $2\gamma K_{\mu 3}$ category was measured with an image plane digitizer to reconstruct the "kink $+2\gamma$" topology in space. A knowledge of $\vec{P}_K$ and the unit vectors $\hat{p}_{\pi+}$, $\hat{p}_{\gamma 1}$, $\hat{p}_{\gamma 2}$ led to a two-constraint fit to the hypothesis $K^+ \to \pi^+\pi^0$. A plot of the two-body χ^2 is shown in Fig. 3. For the purpose of determining the branching ratios a cut was made at $\chi^2 = 30$ to separate $K_{\pi 2}$ and $K_{\mu 3}$ events, and corrections were made for the misidentified events in the two samples.

Two essential steps were required to transform the numbers of events given in Table I, together with $K_{\pi 2}$-$K_{\mu 3}$ separation based on two-body χ^2, into the branching ratios given in Table II. First, the efficiency of the apparatus to the detection of the various decay modes had to be calculated using Monte Carlo techniques. Second, some rearrangement of the event classifications was necessary. The Monte Carlo calculation had two parts: (a) prediction of the fraction of charged secondaries resulting from K^+ decays in the fiducial volume which were removed by the veto counter A_2, which varied somewhat from mode to mode resulting in a mode-dependent trigger efficiency, and (b) prediction of the probability that a π^0 had less than two γ rays which converted in the shower chamber. Because of the rich data sample with 1γ, 2γ, 3γ, and 4γ events, numerous cross checks on the shower theory calculations were available.

The rearrangement of the event classification was complicated since events removed from one category were transferred to another. A two-dimensional array illustrating this process is shown in Table III for the 2γ events. The first two columns are the total number of $K_{\mu 3}$ candidates sorted into $\chi^2 < 30$ and $\chi^2 > 30$. After this separation various small corrections were applied. Of the 12 405 events with $\chi^2 < 30$, 199 were taken to be $K_{\mu 3}$ on the basis of Monte Carlo calculations of the number of $K_{\mu 3}$ events expected to fit the $K_{\pi 2}$ hypothesis. Of the 2485 events with $\chi^2 > 30$, 339 were assigned to other categories leaving 2146 $K_{\mu 3}$'s. Shower theory Monte Carlo technique was used to estimate the 95 2γ τ'. The $K_{\pi 2}$'s with $\chi^2 > 30$ could have been estimated from the tail of the χ^2 distribution, but this was felt to be unreliable because of the non-Gaussian nature of the errors. Instead the distribution in decay angle θ in the lab was used to estimate the $K_{\pi 2}$ contamination from its "Jacobian peak". In this manner 109 events were assigned to $K_{\pi 2}$. Figures 4(a) and 4(b) show the distributions used to obtain this number. The 65 foils were estimated from data taken with the amount of aluminum in between counters A_1 and A_2 increased by a factor of two. The 70 low-energy e's which did not shower were also obtained from Monte Carlo studies. The fourth column contains the $2\gamma e$'s. Of the 3539 events, an excess of 93 appeared to have good two-body χ^2, and were taken to be $K_{\pi 2}$

TABLE III. Branching-ratio data 2γ event rearrangement.

Assigned Categories / Initial Categories	$K_{\mu 3}$ candidates $\chi^2 < 30$	$K_{\mu 3}$ candidates $\chi^2 > 30$	π^* $K_{\pi 2}$	$2\gamma e$	
	12 405	2485	3798	3539	Totals
$\pi^+\pi^0$	12 206	109	3779	93	16 187
$\mu^+\pi^0\nu$	199	2146	···	···	2345
$e^+\pi^0\nu$	···	70	···	3446	3516
$\pi^+\pi^0\pi^0$	···	95	19	···	114
foil interaction	···	65	···	···	65

in which the π^+ faked a shower, presumably by charge exchange in the steel with a conversion of one of the π^0 γ rays in the forward direction. To obtain the re-sorted numbers of two γ events, the numbers in the final category rows were added, giving the results shown in the right-hand column in Table III and also in the second column of Table II. The number of $K_{\mu 2}$ shown in Table II has been decreased by 966 events from the 63 110 $K_{\mu 2}$ events found by the film scan. Two components made up these 966 events -0γ $K_{\pi 2}$ and $K_{\mu 3}$, calculated from shower theory, and events in which the K^+ scattered in between counters A_1 and A_2, producing no visible recoils. These numbers were checked by measuring 10 000 $K_{\mu 2}$ events and comparing the observed muon range in steel with that expected on the basis of $K_{\mu 2}$ kinematics.

The errors shown in Table II reflect uncertainties in the treatment of the various backgrounds and in the Monte Carlo calculations of the detection efficiencies as well as statistical errors. The errors quoted for the various K^+-decay branching fractions compare well with the errors assigned to the world averages, except for the mode $K^+ \to \pi^+\pi^+\pi^-$, where the error quoted here is considerably larger due to the sensitivity of the τ-detection efficiency to the precise size and location of the veto counter A_2. The apparatus had essentially uniform detection efficiency over 87% of the allowed $K_{\mu 3}$ phase space and 90% of the allowed K_{e3} phase space. As a result these branching fractions are particularly insensitive to the values of the form factors describing these decays. Another strong feature of these data is that all branching fractions come from a single sample of K^+ decays rather than from averages of many different experiments in which the partial decay modes were measured separately.

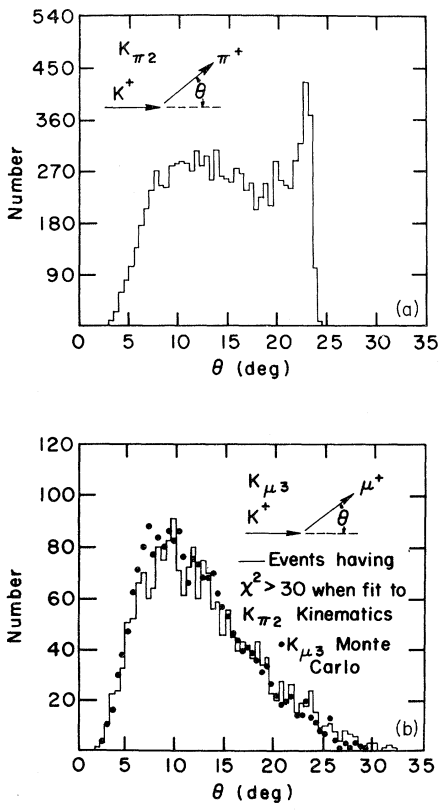

FIG. 4. (a) Distribution in lab angle θ for the π^+ from $K^+ \to \pi^+\pi^0$ decay in flight. Note the strong peak at the kinematic maximum angle. (b) The same plot for the $K_{\mu 3}$ events, compared with the Monte Carlo expectation for pure $K_{\mu 3}$ decay. The remaining $K_{\pi 2}$ contamination was estimated by comparing these two graphs.

III. DATA REDUCTION - THREE-BODY SEMILEPTONIC MODES

A second portion of the film was scanned to obtain a sample of K^+_{e3} and $K^+_{\mu 3}$ events which could be reconstructed in the K^+ rest frame so that the three-body phase space distributions could be studied. The scanning rules were similar to those discussed in Sec. II, but there were certain differences. The full visible decay path between counters A_1 and A_2 was used to obtain the largest possible data sample. Also a slightly different emphasis was placed on event selection. Every event had to be accounted for in the scan for the branching-fraction measurement, but this requirement was relaxed in the three-body distribution studies in favor of obtaining leptonic samples with as high purity as possible. This selectivity resulted in the depletion of certain topologies of events. Examples were K_{e3} events with very low energy nonshowering positrons; and K_{e3} events with a good positron shower and one high-energy γ-ray shower, which tended to obscure a second low-energy γ ray. The basic event classification was made as in Sec. II. K_{e3} events were identified by appearance: two converting γ rays and a positron shower. The shower requirement eliminated from the sample K_{e3} events with positron laboratory energy less than 100 MeV, corresponding to about 3% of the positrons in a 35° forward cone. $K_{\mu 3}$ events were identified by measuring the space angles of the γ rays and the straight "muon" track for each $K_{\mu 3}$ candidate, and then making a $K_{\pi 2}$-$K_{\mu 3}$ separation based on two-body χ^2. In this manner 4232 $K_{\mu 3}$ events and 5497 K_{e3} events were selected.

Some information regarding the consistency of an event with the K_{l3} hypothesis could be obtained from the space angles alone. These data were not sufficient, however, to allow reconstruction of the events in the K^+ rest frame. In order to do the

reconstruction and to eliminate the remaining contaminations in the data a constrained fit to the three-body decays had to be performed. With no knowledge of the neutrino, a two-constraint fit to K_{l3} was possible if the energy of the lepton and the energies of the two γ's were known. The muon energy for $K_{\mu 3}$ was measured from its observed range in steel. The energies of the γ rays and positrons had to be inferred from the information contained in the electromagnetic showers. The $K_{\pi 2}$'s furnished a large sample of γ rays in the shower chamber with known energy, and thus served to calibrate the γ-ray energy measurements. The energy range covered by γ rays in the laboratory from $K_{\pi 2}$, K_{e3}, and $K_{\mu 3}$ decays were all very similar. No direct information on positron showers was available, so the determination of the lepton energy in K_{e3} was the least certain part of the three-body reconstruction.

Roughly 20 000 events previously fitted to the $K_{\pi 2}$ hypothesis were involved in the calibration of the shower chamber and in the measurement of the lepton and γ-ray energies. To save time the measurer estimated the shower energies rather than actually counting the number of sparks. A continuous check of the calibration of the γ-energy estimates was maintained throughout the data analysis by having the measurer read the fitted γ-ray energies for the $K_{\pi 2}$'s immediately after recording his own estimation. A systematic error and width as a function of E_γ was calculated from the $K_{\pi 2}$ estimates. These uncertainties are shown schematically in Fig. 5. The error distribution for estimates at fixed E_γ was approximately Gaussian. A spark count on 2000 $K_{\pi 2}$ events verified that this technique was comparable to spark counting. For γ-ray energies up to 1.4 GeV/c, the number of sparks was given roughly by E_γ (MeV) $= 8 \times$(number of sparks). A similar procedure was used to calibrate the estimates of the positron energy in K_{e3} decay.

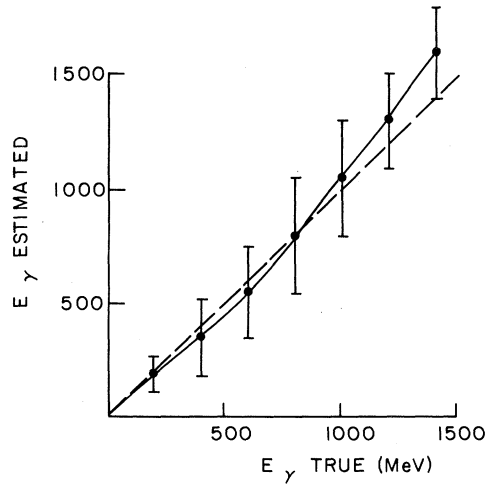

FIG. 5. Illustration of the systematic error and standard deviation of the γ energy estimates as a function of the true γ-ray energy for $K_{\pi 2}$ events.

After measuring the muon range and estimating the γ-ray energies and the positron energy, the 4232 $K_{\mu 3}$'s and 5497 K_{e3}'s were analyzed by the three-body reconstruction programs. Monte Carlo techniques were used to estimate that 5% of the true $K_{\mu 3}$'s and 3% of the true K_{e3}'s would fail to satisfy the three-body fitting routines due to measurement errors. More muon events would fail than positron events because of tighter space angle requirements. Actually 573 $K_{\mu 3}$'s (13.5%) and 213 K_{e3}'s (3.9%) were eliminated for failure to satisfy three-body kinematics, leaving 3659 $K_{\mu 3}$ and 5284 K_{e3} events. This procedure therefore eliminated 360 background events from the $K_{\mu 3}$ data, and 50 background events from the K_{e3} data. More Monte Carlo study showed that approximately 179 background events, composed of 110 $2\gamma\tau'$, 17 nonshower K_{e3}'s, and 52 $K_{\pi 2}$ with an invisible π-μ decay in flight remained in the $K_{\mu 3}$ data. These backgrounds could not be removed on an event by event basis. Therefore the $K_{\mu 3}$ sample obtained by scanning and two-body χ^2 analysis had a 539 event background. This purification procedure can be compared with the one used to eliminate backgrounds on a statistical basis in Table III. In that case 339 background events were subtracted from an initial sample of 2485 $K_{\mu 3}$'s, which would scale to 580 events from 4232 $K_{\mu 3}$'s. This good agreement shows that the three-body reconstruction employed here and the background subtractions employed in Sec. II served the same purpose.

IV. $K^+ \to \pi^0 e^+ \nu$

The most general form for the weak-interaction Hamiltonian for $K^+ \to \pi^0 e^+ \nu$, setting $m_e = 0$ and assuming locality of the leptonic weak vertex is

$$H_w = \frac{G \sin\theta}{\sqrt{2}} \Big[V_\alpha \bar{\psi}_e \gamma_\alpha (1+\gamma_5) \psi_\nu + M_K f_S(q^2) \bar{\psi}_e (1+\gamma_5) \psi_\nu + i \frac{f_T(q^2)}{M_K} (P_\alpha^\pi P_\beta^K - P_\beta^\pi P_\alpha^K) \bar{\psi}_e \sigma_{\alpha\beta} (1+\gamma_5) \psi_\nu \Big] . \quad (1)$$

Here the first term is the usual vector part $V_\alpha = f_+(q^2)(P_\alpha^\pi + P_\alpha^K)$, and $f_S(q^2)$ and $f_T(q^2)$ are the possible scalar and tensor form factors, respectively. M_K is the K^+ rest mass. P_α^K and P_α^π are the components of the four-momentum of the K^+ and π^0. The variable q^2 is the invariant mass squared of the $e\nu$ system:

$$q^2 = (P_\alpha^e + P_\alpha^\nu)(P_\alpha^e + P_\alpha^\nu)$$
$$= M_K^2 + m_\pi^2 - 2M_K E_\pi . \quad (2)$$

If the form factors f_S and f_T are set equal to zero – an assumption consistent with experiment – then the decay depends only on one form factor, $f_+(q^2)$. Since q^2 and E_π are linearly related, the π^0 energy distribution contains all the dependence of the decay on $f_+(q^2)$. Under these assumptions the density distribution on the Dalitz plot has the form

$$\rho(E_\pi, E_e) = |f_+(q^2)|^2[2E_e E_\nu - M_K(W_\pi - E_\pi)] \quad (3)$$

apart from an over-all normalization. Here $E_\nu = M_K - E_\pi - E_e$, and the maximum allowable pion energy $W_\pi = (M_K^2 + m_\pi^2)/2M_K$.

It was pointed out by Marateck and Rosen[5] that rather than the two variables (E_π, E_e), some advantages could be obtained by using the variables $(\cos\beta, V^2)$, where β is the angle between the positron and the neutrino in the π-ν center-of-mass frame, and $V^2 = M_K^2 - 2M_K E_e$ is the invariant mass squared of the π-ν system. Since the range of $\cos\beta$ is $-1 \leq \cos\beta \leq +1$ regardless of the value of V^2, the Dalitz-plot boundary is rectangular, which can be very useful. For example, the dependence of the density $\rho(\cos\beta, V^2)$ on $\cos\beta$ is preserved when integrated over all values of V^2. In terms of these variables, Eq. (3) has the form

$$\rho(\cos\beta, V^2) = |f_+(q^2)|^2 \times \frac{(V^2 - m_\pi^2)^2(M_K^2 - V^2)^2}{V^2}(1 + \cos\beta), \quad (4)$$

where

$$q^2 = (V^2 - m_\pi^2)(M_K^2 - V^2)(1 - \cos\beta)/(2V^2) .$$

Note that $\rho(\cos\beta = -1, V^2) = 0$. This is a property of the vector weak interaction in the limit $m_e \to 0$; antiparallel leptons are forbidden.

The dependence of $f_+(q^2)$ on q^2 can be left arbitrary, or can be parametrized by a single pole term of an unsubtracted dispersion relation

$$f_+(q^2) = \frac{f_+(0)}{(1 - q^2/M_+^2)} . \quad (5)$$

The mass M_+ would be that of a low-lying strange vector meson, presumably the $K^*(890)$. For K_{e3} decay the allowed range of q^2 is $0 \leq q^2 \leq 0.129$ GeV^2. Since $M_{K^*}^2 = 0.79$ GeV^2, the q^2 term in the denominator is expected to remain less than ~0.2. Therefore a linear expansion for $f_+(q^2)$ is often used,

$$f_+(q^2) = f_+(0)(1 + \lambda_+ q^2/m_\pi^2), \quad (6)$$

where the dimensionless parameter $\lambda \approx m_\pi^2/M_+^2$ has been introduced.

In order to compare the 5284 K_{e3} events with Eqs. (3) or (4), Monte Carlo techniques had to be used to generate the expected distributions as distorted by the experimental apparatus and the reconstruction programs. As discussed in Sec. III, the initial scan tended to lose data at low positron and γ-ray energies. To eliminate possible bias, cuts were made by requiring $E_e > 150$ MeV and $E_\gamma > 100$ MeV. Further cuts on the laboratory energies had no effect on the results. Since the distribution in π^0 energy in the center-of-mass system contains virtually all of the information in K_{e3} decay, it is worth noting that after the low-energy γ rays were eliminated the detection efficiency of the apparatus was not dependent on E_γ. A sample of 4017 events remained. The over-all efficiency of the apparatus for detecting these events was calculated to be 0.397, so this corresponded to 10 118 K_{e3} decays in the fiducial volume between counters A_1 and A_2. This number will be used in Sec. V to calculate the branching ratio $K_{\mu 3}/K_{e3}$.

These 4017 K_{e3} events were compared with Monte Carlo data generated according to $A = 2E_e E_\nu - M_K(W_\pi - E_\pi)$ in Eq. (3) and to $q^2 A$, giving a fit to the parameter λ_+ defined by Eq. (6). The A term and the $q^2 A$ term were also transformed into the $(\cos\beta, V^2)$ variables and a fit again performed to obtain λ_+. This essentially represents a different binning in the χ^2 analysis. Since the most sensitive energy variable is E_π, a value of λ_+ could be obtained from the opening angle distribution of the γ rays alone. This latter analysis had the advantage of being independent of the γ-ray and positron energy measurements, but had somewhat larger standard deviation errors. All of the χ^2 values were satisfactory. These results are collected in Table IV. The fitted distributions projected on the q^2/m_π^2 axis and the $\cos\beta$ axis are shown in Figs. 6 and 7, respectively. Note that distortions of the data sample by the apparatus were not severe. For example, the $\cos\beta$ distribution is nearly linear with a very small intercept at $\cos\beta = -1$, in agreement with Eq. (4) for constant form factor λ_+. A nonzero λ_+ adds a term proportional to $(1 - \cos^2\beta)$ to the distribution. Similarly the distribution in q^2 is well behaved except

TABLE IV. Fits to λ_+ in $K^+ \to \pi^0 e^+ \nu$. 4017 events.

Method	λ_+ [a]	$\pm\Delta\lambda_+$	M_+(MeV) [b]	χ^2	$\langle\chi^2\rangle$
$\rho(E_\pi, E_e)$	0.030	0.011	808	77	61
$\rho(\cos\beta, V^2)$	0.029	0.011	822	86	64
$\gamma\gamma$ opening angle	0.031	0.013	796	36	37

[a] Dimensionless parameter λ_+ defined by Eq. (6).
[b] Mass of the exchanged vector meson $M_+ = m_\pi(\lambda_+)^{-1/2}$.

for the highest q^2 point. The data did not require q^4 terms in the distribution to give a satisfactory fit.

No radiative corrections have been applied to the results quoted in Table IV. Theoretical discussion of radiative corrections to K_{e3} decay has been presented by Ginsberg.[6] There are two types of corrections: (a) virtual diagrams, giving corrections to $\pi^0 e^+ \nu$ final state; and (b) real inner bremsstrahlung diagrams, leading to the 4-body final state $K^+ \to e^+ \pi^0 \gamma \nu$. The virtual diagrams contribute a term proportional to α/π to the weak Hamiltonian [Eq. (1)] which depends only on E_e, or V^2 in terms of the Marateck-Rosen variables. Because of the rectangular Dalitz plot in (V^2, cosβ) space, integration over V^2 does not affect the distribution in cosβ, so a measurement of λ_+ by fitting the distribution in cosβ, as shown in Fig. 7, gives a result independent of these virtual corrections. For decays where a real γ ray is emitted, the amount of $e\pi\gamma\nu$ data included in the $e\pi\nu$ sample depends on the method of kinematic reconstruction of the three-body decay, or the allowable range of invariant masses of the ($\nu\gamma$) system which would still be considered $e\pi\nu$ within the experimental resolution. Ginsberg (Ref. 6) made the specific assumption that (E_π, E_e) were known, but no momentum balance information was available. By requiring the (E_π, E_e) point to lie within the three-body phase-space boundary, a limit on the invariant mass of the $\nu\gamma$ system was obtained, which served as the upper limit in the integrals over inner bremsstrahlung. In this experiment the total energy $E_\gamma + E_e$ was observed in the shower chamber. Thus in the three-body reconstruction the presence of real γ rays tended to alter the K_{e3} rate, but had little effect on the Dalitz-plot point. Because of cancellations over the entire Dalitz plot, the change in rate is less than $\frac{1}{2}$%, which is the order of the uncertainty caused by the ultraviolet cutoff.

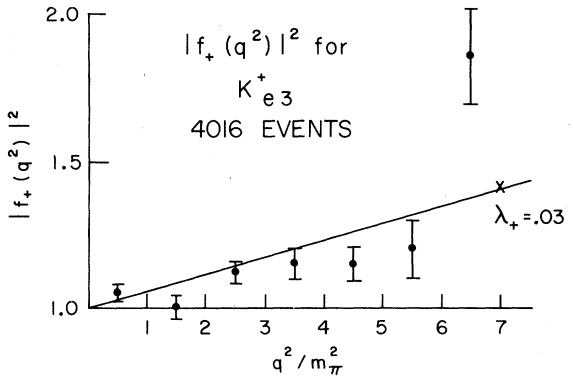

FIG. 6. K_{e3} data as a function of q^2/m_π^2, showing the variation of the form factor.

The best value of λ_+ was taken to be $\lambda_+ = 0.029 \pm 0.011$, as determined by the (cosβ, V^2) Dalitz-plot analysis. Fits were then performed to $|f_S/f_+|^2$ and $|f_T/f_+|^2$ in turn, using Eq. (1). First let $f_T = 0$. Then in terms of (cosβ, V^2) the distribution has the form

$$\rho(\cos\beta, V^2) = \frac{(M_K^2 - V^2)^2 (V^2 - m_\pi^2)^2}{V^4} |f_+(q^2)|^2 \times \left[\left| \frac{f_S}{f_+} \right|^2 (1 - \cos\beta) + \frac{V^2}{M_K^2} (1 + \cos\beta) \right]. \tag{7}$$

The coefficient $|f_S/f_+|^2$ was assumed independent of q^2. For $\lambda_+ = 0.029$, the fit to $|f_S/f_+|^2$ gave

$$\left| \frac{f_S}{f_+} \right|^2 = 0.004 \pm 0.007, \tag{8}$$

where the standard deviation error corresponded to an increase in χ^2 by unity. Defining 90% confidence to be 1.75 standard deviations on a normal error curve, this result can be expressed as

$$\left| \frac{f_S}{f_+} \right| < 0.13 \quad (90\% \text{ confidence}). \tag{9}$$

Some correlation was present between values of λ_+ and $|f_S/f_+|^2$. A 1-standard-deviation increase in λ_+ resulted in approximately a $\frac{1}{2}$-standard-deviation decrease in $|f_S/f_+|^2$.

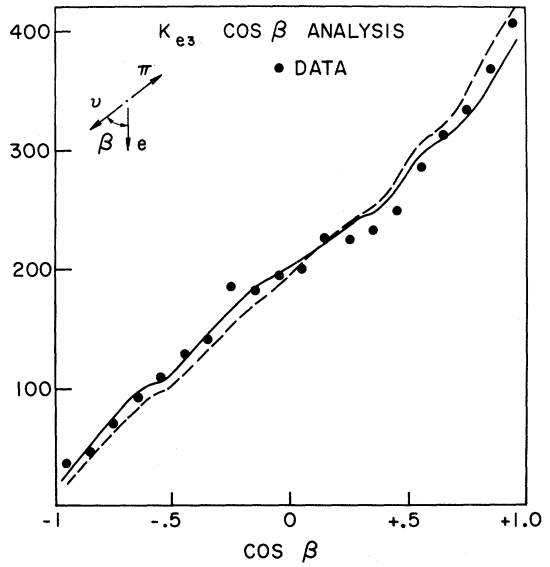

FIG. 7. Same K_{e3} data as in Fig. 6 plotted as a function of cosβ, the angle between e and ν in the π-ν center-of-mass system. The solid curve is the Monte Carlo result for $\lambda_+ = 0.029$, and the dashed curve is for $\lambda_+ = 0$, both normalized to 4017 events. This plot is especially useful for the detection of a scalar form factor f_S.

To estimate $|f_T/f_+|^2$, let $f_S=0$. The formula then is

$$\rho(\cos\beta, V^2)=\frac{(M_K^2-V^2)^2(V^2-m_\pi^2)^2}{V^4}|f_+(q^2)|^2 \times\left[\left|\frac{f_T}{f_+}\right|^2 A^2(1-\cos\beta)+\frac{V^2}{M_K^2}(1+\cos\beta)\right], \tag{10}$$

with

$$A=\frac{1}{2}\left\{1+\frac{V^2}{M_K^2}-\frac{V^2-m_\pi^2}{V^2}\left[1-\frac{M_K^2-V^2}{2M_K^2}(1+\cos\beta)\right]\right\}. \tag{11}$$

The coefficient $A=(E_e-E_\nu)/M_K$. The poor resolution in the positron energy effectively integrated over V^2, which greatly suppressed the experimental sensitivity to $|f_T/f_+|^2$ compared to that for the scalar form factor. Assuming $\lambda_+=0.029$ gave

$$\left|\frac{f_T}{f_+}\right|^2=0.17\pm0.23\,. \tag{12}$$

With the same definitions of errors as before, the form factor ratio limit is

$$\left|\frac{f_T}{f_+}\right|<0.75 \quad (90\%\text{ confidence})\,. \tag{13}$$

Thus, the data do not require a tensor term, but do not strongly discriminate against one.

The $X2$ collaboration has recently performed an analysis using $K^+_{\mu3}$ and branching ratio data and quotes $|f_S/f_+|<0.15$, $|f_T/f_+|<0.22$ both at the 68% confidence level.[7] A review by Rubbia in 1969 quotes averages of $|f_S/f_+|<0.2$ and $|f_T/f_+|<0.58$ at the 90% confidence level.[8] The results obtained in this experiment thus place a new upper limit on the scalar form factor.

V. $K^+\to\pi^0\mu^+\nu$

In order to allow for the finite mass of the muon, the vector current V_α in Eq. (1) must be modified:

$$V_\alpha=f_+(q^2)(P^K_\alpha+P^\pi_\alpha)+f_-(q^2)(P^K_\alpha-P^\pi_\alpha)\,.$$

For simplicity both $f_S(q^2)$ and $f_T(q^2)$ were set equal to zero. Defining the form factor ratio $\xi(q^2)=f_-(q^2)/f_+(q^2)$, and taking $\mathrm{Im}[\xi(q^2)]=0$ gives the $K_{\mu3}$ density formula

$$\rho(E_\pi, E_\mu)=|f_+(q^2)|^2[A(E_\pi, E_\mu)+B(E_\pi, E_\mu)\xi+C(E_\pi)\xi^2]\,. \tag{14}$$

The terms inside the square brackets are

$$A=2E_\mu E_\nu-M_K(W_\pi-E_\pi)+\frac{1}{4}\frac{m_\mu^2}{M_K}(W_\pi-E_\pi)-\frac{m_\mu^2}{M_K}E_\nu,$$
$$B=\frac{m_\mu^2}{M_K}[E_\nu-1/2(W_\pi-E_\pi)]\,, \tag{15}$$
$$C=\frac{1}{4}\frac{m_\mu^2}{M_K}(W_\pi-E_\pi)\,.$$

The notation is the same as in Eq. (3). A linear parametrization of the q^2 dependence of f_+ and f_- leads to

$$f_+(q^2)=f_+(0)(1+\lambda_+q^2/m_\pi^2)$$
and
$$\xi(q^2)=\xi(0)[1+(\lambda_--\lambda_+)q^2/m_\pi^2]\,. \tag{16}$$

This λ_+ and the one in Eq. (6) for K_{e3} analysis should be the same if μ-e universality is valid.

The final sample of 3659 $K_{\mu3}$ decays contained 179 background events as discussed in Sec. III. Monte Carlo distributions for these backgrounds in addition to the Monte Carlo distributions for A, B, C, and q^2A were used in the fit of the data to Eq. (14). Fixing $\lambda_+=\lambda_-=0.029$ gave the result

$$\xi(0)=-0.09\pm0.28\,,$$
$$\chi^2=54(53)\,. \tag{17}$$

A perspective view of the events on the (E_π, E_μ) Dalitz plot is shown in Fig. 8. No cuts have been made on the plot, and the data populate the area in an essentially distortion-free manner. Only the very lowest kinetic-energy muons are missing, because of the veto counter A_2.

A fit to $\xi(q^2)$ can be obtained independent of $|f_+(q^2)|^2$ by dividing the data into bins in q^2, and by leaving the normalization in each bin free. This technique makes no assumptions concerning the form of the q^2 dependence of ξ, and yields $\xi(q^2)$ independent of λ^+. It is the analog of the $\xi(q^2)$ obtained by measuring the muon polarization. The fit depends on the shapes of the A, B, and C terms in Eq. (15). At fixed q^2 the distribution in E_μ is written

$$\rho_{q^2}(E_\mu)=\frac{N_{q^2}[A_{q^2}(E_\mu)+B_{q^2}(E_\mu)\xi+C_{q^2}\xi^2]}{\int A_{q^2}\,dE_\mu+\xi\int B_{q^2}\,dE_\mu+\xi^2C_{q^2}\int dE_\mu}\,. \tag{18}$$

Here N_{q^2} is the number of events in that q^2 bin, and the denominator ensures proper normalization regardless of the value of ξ. Seven bins in q^2 were chosen and the results for $\xi(q^2)$ are shown in Fig. 9(a). Figure 8 shows the data compared with the Monte Carlo predictions for the fits. A fit could

not be obtained in the highest q^2 bin because of the small amount of data (108 events) and the similarity in shape of the three Monte Carlo functions for A, B, and C. The weighted average assuming ξ constant was $\xi = -0.21 \pm 0.35$ in good agreement with Eq. (17). This average value was used to extract $|f_+(q^2)|^2$ from the total amount of data in each bin, and this result is shown in Fig. 8(b). The value of $|f_+(q^2)|^2$ obtained for a particular q^2 bin depends directly on the value previously extracted for $\xi(q^2)$ from the shapes, which illustrates the correlation between ξ and λ^+.

Monte Carlo techniques were used to calculate an efficiency of 0.493 for the detector system and the analysis programs used in processing the $K_{\mu 3}$ events. Taking the net $K_{\mu 3}$ yield to be 3480 events, this scales to 7059 $K_{\mu 3}$ decays. Combining this with the 10 118 K_{e3} decays similarly obtained in Sec. III gives a branching ratio

$$R = \Gamma(K^+ \to \mu^+ \pi^0 \nu)/\Gamma(K^+ \to e^+ \pi^0 \nu) = 0.698 \pm 0.025 .$$

The statistically independent result given in Table III is $R = 0.685 \pm 0.036$. The combined value for this experiment is

$$\frac{\Gamma(K^+ \to \mu^+ \pi^0 \nu)}{\Gamma(K^+ \to e^+ \pi^0 \nu)} = 0.694 \pm 0.022 . \quad (19)$$

Radiative corrections to this ratio are expected to be less than 1% and are uncertain because of the unknown ultraviolet cutoff. Such corrections have not been made.

The parametrized fit quoted in Eq. (17) was obtained by assuming the K_{e3} value for λ_+. If this assumption is relaxed, a somewhat lower χ^2 is obtained with the results $\lambda_+ = \lambda_- = -0.006 \pm 0.015$, $\xi(0) = +0.45 \pm 0.28$, and $\chi^2 = 48(52)$. The branching ratio R depends on $\xi(0)$, λ_+, and λ_- if $\lambda_+(K_{e3})$ and $\lambda_+(K_{\mu 3})$ are taken to be the same. The relation is[9]

$$R = 0.6487 + 0.1269\xi + 0.0193\xi^2 + 1.34\lambda_+ + 0.0077\lambda_+\xi + 0.459\lambda_-\xi + 0.163\lambda_-\xi^2 - 0.068\lambda_+\xi^2 . \quad (20)$$

Figure 10 shows all of the results of this experiment displayed on an ξ-λ_+ graph. The horizontal band is the K_{e3} result $\lambda_+ = 0.029 \pm 0.011$. The branching ratio Eq. (20) gives a relation between ξ and λ_+ which is shown for $R = 0.694 \pm 0.022$. The one- and two-standard-deviation contours come from the free fit to the $K_{\mu 3}$ Dalitz plot quoted

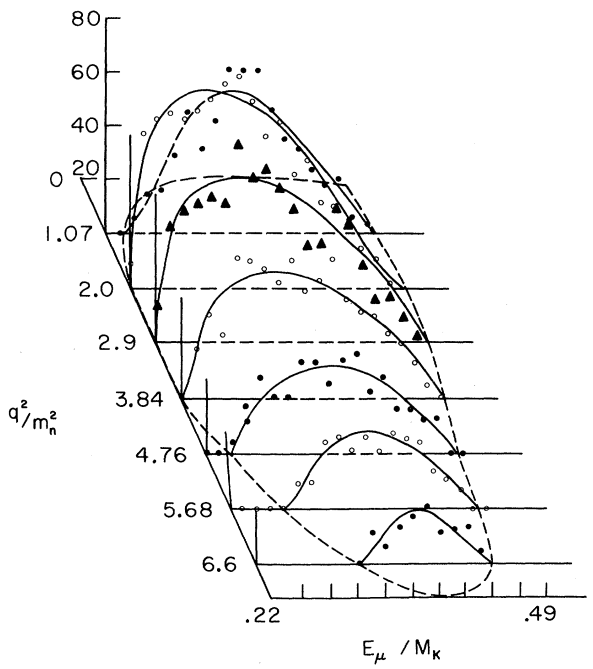

FIG. 8. Perspective view of the $K_{\mu 3}$ data binned according to q^2. The data are displayed as alternating closed and open circles in the first four q^2 bins. The last three bins are triangles, open circles, and closed circles, respectively. The smooth curves are the fits obtained from the unparametrized fit to $\xi(q^2)$, Eq. (18) in the text. The curve for the highest q^2 bin is $\xi = 0$.

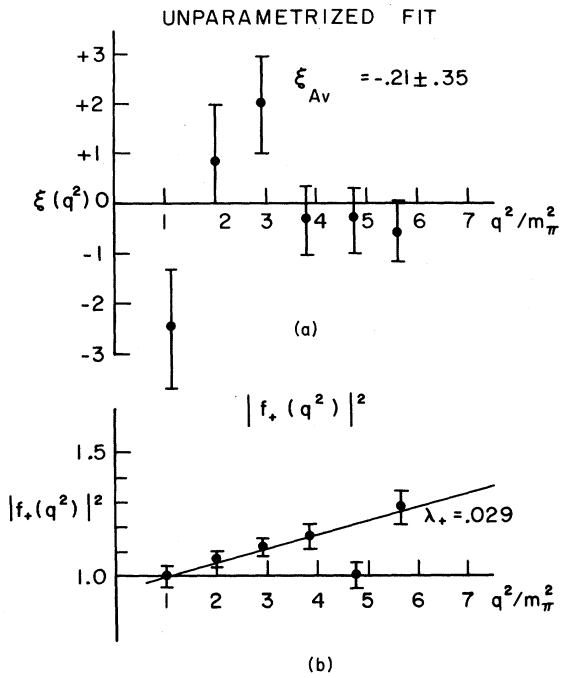

FIG. 9. (a) Results of the unparametrized fit to $\xi(q^2)$. The highest q^2/m_π^2 bin in Fig. 8 could not be fitted because of lack of sensitivity to ξ. The weighted average assuming ξ has no q^2 dependence is $\xi = -0.21 \pm 0.35$. (b) The form factor $|f_+(q^2)|^2$ extracted from the $K_{\mu 3}$ data assuming $\xi = -0.21 \pm 0.35$. The data were normalized to $q^2/m_\pi^2 = 1$.

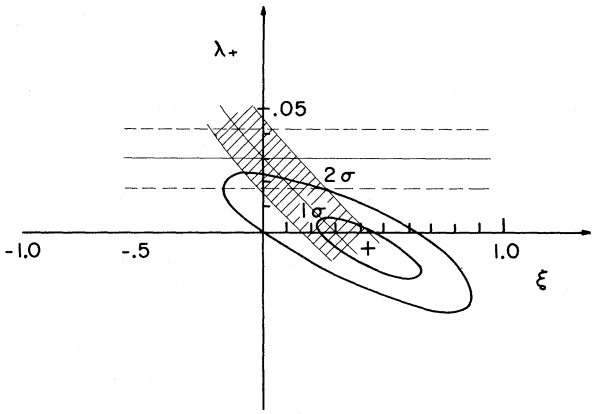

FIG. 10. Summary of the results of this experiment. The K_{e3} results, $\lambda_+ = +0.029 \pm 0.011$, is shown as a horizontal band. The branching ratio result $R = 0.694 \pm 0.022$ is given by the shaded area, and the parametrized fit to the $K_{\mu 3}$ Dalitz plot allowing both ξ and λ_+ to vary is shown by the one- and two-standard-deviation contours.

above. The internal consistency of the various measurements is satisfactory.

VI. DISCUSSION

There have been several recently published measurements of λ_+ in K_{e3} decay.[10-12] The agreement among the various $K_L^0 \to \pi e \nu$ measurements is not very good, but the average, $\lambda_+(K_L^0 \to \pi e \nu) = 0.024 \pm 0.004$ agrees with the charged average value $\lambda_+(K^+ \to \pi e \nu) = 0.029 \pm 0.006$, and with the result quoted in this experiment, $\lambda_+ = 0.029 \pm 0.011$. Such consistency may justify taking a grand average of charged and neutral results, assuming the validity of the $|\Delta \vec{I}| = \frac{1}{2}$ rule in semileptonic decays: $\lambda_+ = 0.026 \pm 0.003$. Similarly, the agreement among the various branching ratio measurements is not bad. The Particle Data Group[2] quotes

$$R_{\text{neut}} = \Gamma(K_L^0 \to \pi \mu \nu)/\Gamma(K_L^0 \to \pi e \nu) = 0.688 \pm 0.018$$

and

$$R_{\text{charged}} = \Gamma(K^+ \to \pi \mu \nu)/\Gamma(K^+ \to \pi e \nu) = 0.659 \pm 0.022 .$$

Combining the latter result with the present experiment gives $R_{\text{charged}} = 0.678 \pm 0.015$. Again assuming the $|\Delta \vec{I}| = \frac{1}{2}$ rule, the average $R = 0.682 \pm 0.011$. These averaged numbers, together with Eq. (20), give $\xi = -0.02 \pm 0.11$.

The picture becomes less clear when other $K_{\mu 3}$ studies are included in the average. Table V shows some recently published studies of $K_{\mu 3}$ decay, including the present experiment. For K^+ decay there has been one muon polarization measurement,[13] one polarization and Dalitz-plot measurement,[7] and the present Dalitz-plot measurement. For K_L^0 decay a large-statistics Dalitz-plot study has been reported.[14] There is no strong evidence for a q^2 dependence to ξ. If λ_+ is allowed to vary its drifts away from the best K_{e3} value, but in all cases μ-e universality is valid to within 1 to 2 standard deviations. Any average of these data would obviously give a negative value for ξ considerably larger in magnitude than the one obtained from average values of λ_+ and R, and also larger than the value found in this experiment alone. Some improvement in the consistency of the results for the various Dalitz-plot experiments can be obtained if the same fixed value of $\lambda_+ = \lambda_-$ is assumed in the analysis of each experiment. The data are not sufficiently precise to determine three or even two correlated parameters in an unambiguous way, but rather a relation among the parameters. The consistency of the experiments lies in the fact that they determine similar relations between ξ and λ_+, but χ^2 prefers different values for the parameters in different experiments, or, indeed in different analyses of the same experiment. The first two results quoted in the table have been analyzed

TABLE V. Recent published $K_{\mu 3}$ results.

Reference	Experiment	Number of events	$\xi(0)$	λ_+	λ_-
7	$K^+ \to \mu^+$ spectrum and polarization	3240	-0.65 ± 0.13 -1.1 ± 0.5	0.029 [a] 0.050 ± 0.018	0.029 [a] 0 [a]
this expt.	$K^+ \to \mu^+$ spectrum	3659	-0.09 ± 0.28 $+0.45 \pm 0.28$	0.030 [a] -0.006 ± 0.015	0.030 [a] $=\lambda_+$
14	$K_L^0 \to \mu^+$ spectrum	16454	-2.3 ± 0.8	$+0.06 \pm 0.02$	-0.15 ± 0.03
13	$K^+ \to$ polarization	3133	-0.95 ± 0.30	...	...

[a] These values were fixed in the fit.

assuming $\lambda_+ = \lambda_- = 0.029$, and together with the fourth entry, a measurement of the muon polarization alone, give an average $\xi(0) = -0.6 \pm 0.14$. The agreement of the third Dalitz-plot experiment with this result is difficult to determine because of the large quoted value for λ_- in their fit. This large value comes essentially from one point on the $\xi(q^2)$ curve, however, and does not contradict the assertion that there is no compelling evidence for a q^2 dependence to ξ.[15]

ACKNOWLEDGMENTS

We wish to thank Dr. F. Schweingruber, Dr. I. Spirn, T. Passi, and the entire ZGS crew for their cooperation in performing the experiment. Some of the apparatus was constructed by Dr. B. Gobbi. Dr. T. Yamanouchi helped during the experimental run. Dr. T. Novey kindly lent the Argonne neutrino spark chambers. The scanning and measuring staffs at Rochester and Wisconsin performed invaluable service.

---

*Work supported in part by the U. S. Atomic Energy Commission under Contract Nos. AT(11-1)-881, COO-881-331, and AT(11-1)-3065.

†Present address: Northwestern University, Evanston, Illinois.

‡Presently at Rockefeller University, New York, New York.

§John Simon Guggenheim Memorial Fellow, 1971–1972.

[1]Theoretical literature: R. E. Marshak, Riazuddin, and C. P. Ryan, *Theory of Weak Interactions in Particle Physics* (Wiley-Interscience, New York, 1969).

[2]Experimental literature: Particle Data Group, Rev. Mod. Phys. 43, S1 (1971), and L. G. Pondrom, in *Particles and Fields–1971,* proceedings of the 1971 Rochester Meeting of the Division of Particles and Fields of the American Physical Society, edited by A. C. Melissinos and P. F. Slattery (A.I.P., New York, 1971), p. 151.

[3]General review: L. M. Chounet, M. K. Gaillard, and J. M. Gaillard, Phys. Reports (to be published).

[4]A more complete description of this phase of the experiment can be found in I. H. Chiang, Ph. D. thesis, University of Rochester, 1971 (unpublished).

[5]S. L. Marateck and S. P. Rosen, Phys. Letters 29B, 497 (1969).

[6]E. S. Ginsberg, Phys. Rev. 162, 1570 (1967); 142, 1035 (1966).

[7]H. Haidt *et al.* (*X*2 Collaboration), Phys. Rev. D 3, 10 (1971).

[8]C. Rubbia, CERN Report No. 69-7 (unpublished).

[9]N. Cabibbo, in *Proceedings of the Thirteenth International Conference on High Energy Physics, Berkeley, 1966* (Univ. of California Press, Berkeley, 1967), p. 29.

[10]C. Y. Chien *et al.*, Phys. Letters 35B, 261 (1971).

[11]H. J. Steiner *et al.* (*X*2 Collaboration) Phys. Letters 36B, 521 (1971).

[12]V. Bisi *et al.*, Phys. Letters 36B, 533 (1971).

[13]D. Cutts, R. Stiening, C. Wiegand, and M. Deutsch, Phys. Rev. Letters 20, 955 (1968).

[14]E. Dally *et al.*, Nuovo Cimento (to be published).

[15]C. Buchanan (private communication).